ADVANCED MATERIALS INTERFACES
www.advmatinterfaces.de

Visible Light Effects on Photostrictive/Magnetostrictive PMN-PT/Ni Heterostructure

Deepak Dagur, Vincent Polewczyk, Aleksandr Yu. Petrov, Pietro Carrara, Marta Brioschi, Sara Fiori, Riccardo Cucini, Giorgio Rossi, Giancarlo Panaccione, Piero Torelli, and Giovanni Vinai*

The possibility of modifying the ferromagnetic response of a multiferroic heterostructure via fully optical means exploiting the photovoltaic/photostrictive properties of the ferroelectric component is an effective method for tuning the interfacial properties. In this study, the effects of 405 nm visible-light illumination on the ferroelectric and ferromagnetic responses of (001) $Pb(Mg_{1/3}Nb_{2/3})O_3$-0.4$PbTiO_3$ (PMN-PT)/Ni heterostructures are presented. By combining electrical, structural, magnetic, and spectroscopic measurements, how light illumination above the ferroelectric bandgap energy induces a photovoltaic current and the photostrictive effect reduces the coercive field of the interfacial magnetostrictive Ni layer are shown. Firstly, a light-induced variation in the Ni orbital moment as a result of sum-rule analysis of x-ray magnetic circular dichroic measurements is reported. The reduction of orbital moment reveals a photogenerated strain field. The observed effect is strongly reduced when polarizing out-of-plane the PMN-PT substrate, showing a highly anisotropic photostrictive contribution from the in-plane ferroelectric domains. These results shed light on the delicate energy balance that leads to sizeable light-induced effects in multiferroic heterostructures, while confirming the need of spectroscopy for identifying the physical origin of interface behavior.

1. Introduction

Multiferroic (MF) heterostructures have been extensively explored over the last decades due to the possibility of controlling both ferromagnetic (FM) and ferroelectric (FE) order across the interface via magnetoelectric coupling.[1–6] This has resulted particularly interesting for technological applications in the case of converse magnetoelectric coupling, i.e., electrically tuning the FM response by an applied bias. The coupling is driven by three main mechanisms: interfacial charge accumulation or depletion (charge-driven), ion migration and strain-mediated effects.[7–11] Despite being a relatively mature field of research and having already reached its technological implementation,[12] the detailed energy landscape of both FE and FM layers needs to be assessed by further investigations, in view of tailoring and optimizing the functionalities. Reversible morphological changes upon polarization[13,14] and fully optical processes[15] are key phenomena to be explored for tuning the interfacial properties.

More generally, these effects exploit the FE materials sensitivity to several external stimuli.[16] Among them, light-induced FE control is a particularly intriguing one and not fully explored yet.[17] Whenever a FE material is illuminated by light with above-bandgap photon energy, free charge carriers are generated across the material via bulk photovoltaic effect (BPVE), which modifies the internal electric field of the sample.[18–21] The superposition in FE materials of BPVE with inverse piezoelectric effect leads to light-induced non-thermal strain in the material (i.e., expansion or contraction under light), known as photostrictive effect,[17,22–26] firstly reported by Tatsuzaki et al. in 1960.[17] The combination of BPVE and inverse piezoelectric effect allows using light to modify the strain in FE, which behaves as a photo-piezoelectric materials. Since then, several studies has focused on photostrictive effects in different FE materials and thin films, for example $Pb_{(1-x)}La_x(Zr_yTi_{(1-y)})_{(1-x/4)}O_3$ (PLZT),[23,27] $BiFeO_3$ (BFO),[26,28,29] and $BaTiO_3$ (BTO),[30] but the renewed attention is currently devoted to $PbTiO_3$ compounds.

D. Dagur, V. Polewczyk, A. Yu. Petrov, P. Carrara, M. Brioschi, S. Fiori, R. Cucini, G. Rossi, G. Panaccione, P. Torelli, G. Vinai
Istituto Officina dei Materiali (IOM)-CNR
Area Science Park, S.S. 14 km 163.5, Trieste I-34149, Italy
E-mail: piero.torelli@elettra.eu
D. Dagur
Department of Physics
University of Trieste
Via A. Valerio 2, Trieste 34127, Italy
P. Carrara, M. Brioschi, G. Rossi
Department of Physics
University of Milan
Via Celoria 16, Milan I-20133, Italy

The ORCID identification number(s) for the author(s) of this article can be found under https://doi.org/10.1002/admi.202201337.

DOI: 10.1002/admi.202201337

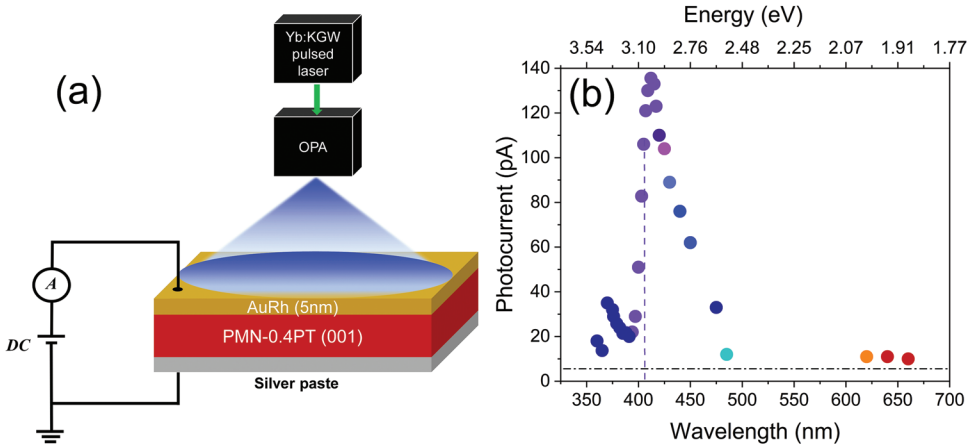

Figure 1. a) Schematic representation of the photocurrent measurements of PMN-0.4PT (001) pristine substrate under variable wavelengths illumination (λ ranging from 360 to 660 nm), produced by OPA. The light fluence was kept constant at all wavelengths at 480 mW cm^{-2}. The sample was illuminated for 2 min on the AuRh capped side. b) Measured photocurrent as the function of wavelength and corresponding photon energies. Vertical dashed line corresponds the photocurrent at 405 nm wavelength, i.e., the photon energy used for continuous illumination. Horizontal line corresponds to the background photocurrent in absence of illumination.

Among all FE materials, $Pb(Mg_{1/3}Nb_{2/3})O_{3-x}PbTiO_3$ (PMN-PT) resulted particularly interesting due to its endurance to polarization switching and low cost.[13,31,32] PMN$_{-x}$PT crystals exhibit variations in structural and electromechanical properties as a function of PT concentration. In the case of PMN-0.4PT, the structure lies near the morphotropic phase boundary and is considered to be tetragonal at room temperature.[33] PT concentration impacts directly the optical properties of PMN-PT crystals,[34–36] with the refractive index increasing with the increase in PT content.[34,37] BPVE directly depends on the refractive index and hence on the band gap energy of FE substrates.[38]

In MF heterostructures, light-induced FE strain modulation proved to be an effective way for tailoring the FM interfacial properties,[15,39–44] not being affected by aging and fatigue processes typical of voltage controlled FE polarization switching.[45] In 2016, Iurchuk et al.[15] reported the optical writing and electrical erasing of the magnetic state for hybrid Au/BFO/Ni structure under the 404 nm laser illumination, with a up to 75% change in coercive field of Ni under irradiation. Concerning PMN-PT/FM heterostructures, very few reports are present at the moment and all characterizations are based on magnetometric and electric measurements. Recently, Zuo et al. showed that UV illumination on PMN-0.3PT (011) induces changes on interfacial Ni magnetic properties,[39] reversibly switching from easy to hard axis in all FE polarization states.

To our knowledge no previous study has addressed the spectroscopic features of the FM layer in MF heterostructures under illumination. We have measured the electronic structure response of the FM layer when photostrictive changes are present in the framework of our electrical, structural, magnetic, and spectroscopic investigation on the light-induced photovoltaic/photostrictive properties of a PMN-0.4PT (001) substrate and on their induced reversible effects on the magnetic properties of an interfacial Ni thin. By tuning the illumination wavelength via an Optical Parametric Amplifier (OPA), we show by electron transport measurements and $I(E)$ curves the BPVE effect in the substrate. By means of Magneto–Optic Kerr Effect (MOKE) magnetometry, we show how light illumination induces modifications on the magnetic coercive field (H_C) as the function of variable light intensity. X-ray magnetic circular dichroism (XMCD) measurements at Ni $L_{2,3}$ edges reveal that under irradiation not only H_C is modified, but the total magnetic moment is reversibly changed. Specifically, the variation of the orbital moment is a direct spectroscopic evidence of the strain changes under illumination, therefore connecting the effects of photostriction and FM response. While in the pristine case the illumination under 405 nm wavelength at 800 mW cm^{-2} induced a 45% H_C reduction, the effect was strongly reduced when polarizing the sample in the out of plane direction. By combining structural and spectroscopic data we hint to that the changes in Ni properties are connected with the photostrictive phenomena taking place in the substrate, whose efficiency is maximum for in-plane FE domains.

2. Results and Discussion

2.1. Photocurrent Characterization on PMN-PT Substrate via OPA

In order to determine the ideal illumination wavelength to maximize the photoinduced effects on PMN-PT, photocurrent measurements were performed as a function of photon energy by using an OPA setup on a PMN-0.4PT (001) substrate. The measurements were recorded by applying a steady voltage of 1 V through the thickness of the sample, measuring the output current. A schematic of the setup is shown in **Figure 1**a. A collimated beam of the same size of the sample substrate (around 2.5 × 2.5 mm^2) was irradiated on the front side of the sample. Figure 1b shows the resulting photocurrent generated under illumination as a function of wavelength (and corresponding photon energies), which was scanned from 360 to 660 nm. The maximum of photocurrent was found in correspondence to a 412 nm wavelength, corresponding to a band gap of 3.01 eV, while a detectable photovoltaic effect was observed in a quite

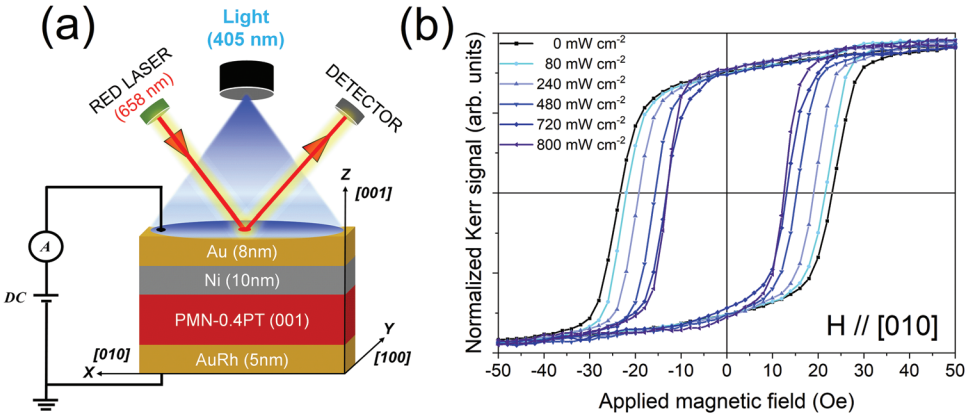

Figure 2. a) Schematic representation of the PMN-0.4PT/Ni heterostructure and experimental setup. A He-Ne laser is used for the MOKE measurements, while a continuous 405 nm laser is illuminating the whole sample surface. b) Hysteresis loops measured with the magnetic field applied along the PMN-PT (010) axis under light illumination of variable power (0–800 mW cm^{-2}).

large range of energies, from 2.61 to 3.35 eV, consistent with the range reported for different PMN$_{-x}$PT crystals.[34] In FE, the photon energy dependence of photoconductivity and hence resulting photostriction is a result of two competitive effects: electric field redistribution, which leads to an increase of the internal polarization field, and electric field screening by the light excited charge carriers, which leads to a decrease of electric field in the sample.[22] These two opposing effects as the function of wavelength determine the amonotonous behavior of photovoltaic/photostrictive effects as in the 2.7–3.6 eV photon energy range, as shown in Figure 1b.

In the following experiments, all the laser illumination on the PMN-PT/Ni heterostructures was done with a continuous 405 nm laser of tunable power. Since BPVE in FE has similar trends under both pulsed and continuous laser illuminations,[46] we consider it to be close to the maximum of photocurrent (Figure 1b) and therefore appropriate for the investigation.

2.2. Light-Induced Effects on the Magnetic Properties of Pristine PMN-PT/Ni

The magnetic properties of pristine PMN-PT/Ni heterostructure were analyzed by MOKE measurements, both without and with light illumination of variable intensity. A schematic representation of the sample stack and experimental setup for MOKE measurements is shown in **Figure 2**a. The crystallographic axis refers to the structural order of the FE substrate. Similar setups are reported in literature with the illumination either on the backside electrode[39] or on the side.[47] Polar measurements showed an in-plane almost isotropic behavior as shown in (Figure S1, Supporting Information), with a coercive field H_C of around 19 Oe width along the [100] axis and 23 Oe along the [010] one. The effects of light illumination for the case of magnetic field H // [010] is shown in Figure 2b. A large H_C reduction was detected under illumination, with increasing effects as a function of irradiance, up to 45% under light illumination of 800 mW cm^{-2}, while the changes in magnetic remanence were negligible. We underline that the hysteresis loops presented in Figure 2b are normalized to the magnetic saturation of each curve, so changes in the total magnetization under illumination are here not visible. The loop was also measured under red laser (653 nm) illumination of 128 mW cm^{-2} and we see no changes in the loop, proving that the red laser has no impact in changing the magnetic properties of Ni.

These magnetic changes are fully reversible and reproducible, with the magnetic signal fully restored after switching the laser off (Figure S2, Supporting Information).

After MOKE characterizations, XMCD measurements were carried out at the APE-HE beamline of NFFA on the Elettra synchrotron radiation source to determine the magnetic changes of the Ni thin film under illumination. As part of the laser light was absorbed by the viewport window of the UHV endstation, the effective illumination power on the sample was 700 mW cm^{-2}. The XAS spectra at Ni $L_{2,3}$ edges revealed a partial oxidation of the layer, with features that we attribute to a small surface NiO contribution (Figure S3, Supporting Information).[48] Since no spectral evolution was observed along the whole set of measurements, we consider the Ni layer chemically stable in all the studied conditions, excluding the possibility of any ion migration from/to the substrate (Figure S4, Supporting Information). In **Figure 3**, we show

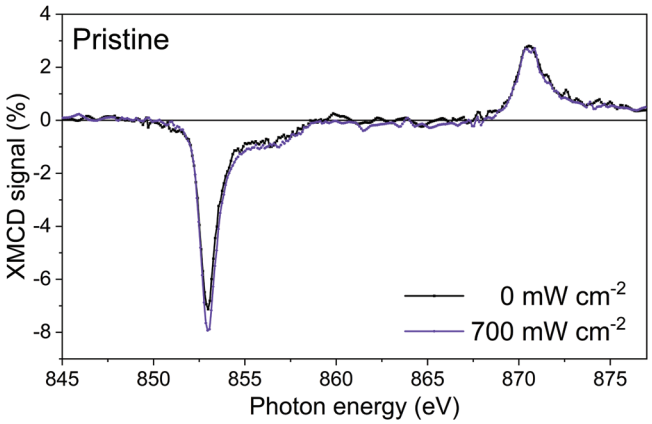

Figure 3. XMCD dichroic signal at Ni $L_{2,3}$ edges in case of pristine PMN-PT/Ni, in absence and presence of light of 700 mW cm^{-2}, applying the magnetic field along [010].

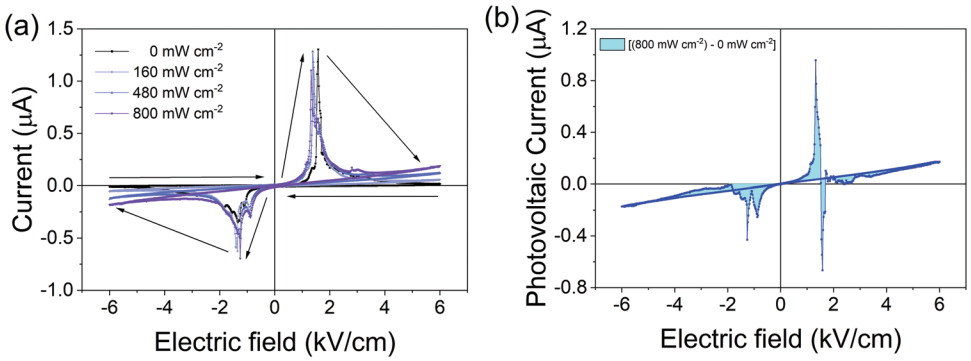

Figure 4. a) $I(E)$ curves of the PMN-PT/Ni heterostructure under continuous 405 nm laser illumination of variable power (0–800 mW cm^{-2}) and b) the photovoltaic current generated in PMN-0.4PT (001) substrate, obtained by subtracting the curve taken with no light from the one under 800 mW cm^{-2} illumination.

the XMCD spectra with and without 405 nm illumination for the pristine PMN-PT case, averaged over three different zones of the sample (see Figure S5, Supporting Information). The spectra show an L_3 edge XMCD intensity of (7.1 ± 0.1)% with no light and (7.9 ± 0.1)% under illumination. Interestingly, the dichroic signal at L_2 edge does not change. This is a signature of a change of the Ni electronic properties induced by photostriction of the substrate, as it indicates a change of the Ni orbital moment.[49]

By applying the XMCD sum rules to the measured spectra,[50,51] we derived the spin (m_{spin}) and orbital (m_{orb}) magnetic moments of Ni in absence and presence of light illumination for the data presented in Figure 3. It results that the ratio m_{orb}/m_{spin} was found to be 0.0940 with no light and 0.1149 under illumination. The change in this ratio for Ni represents the interface induced effect by PMN-PT photostriction when under illumination.

2.3. Photocurrent Effects on Pristine and Polarized PMN-PT/Ni

PMN-PT/Ni was polarized by applying an electric voltage up to ±6 kV cm^{-1} through the thickness of the sample. **Figure 4**a shows the $I(E)$ curves under different illumination intensities, with the setup shown in Figure 2a, sweeping the electric field along the [001] crystallographic direction from −6 to +6 kV cm^{-1} and then back to zero, in presence and absence of 405 nm light illumination. Stable and reproducible FE transitions were recorded around ±1.5 kV cm^{-1}, consistently with what previously reported by our group on similar substrates.[13,14] Light illumination induces a significant change in the curves, with an additional linear slope as a function of the applied bias, whose intensity increases with illumination. The presence of this slope is a clear sign of free charge carrier generation in the sample, i.e., induction of BPVE.[26,47] The photovoltaic current induced in the sample under 800 mW cm^{-2} illumination as the function of electric field, given by the difference between $I(E)$ under illumination and no light, is shown in Figure 4b. This difference helps in understanding the effects of light illumination on PMN-PT during the polarization switching. Specifically, two main effects can be noticed here: i) a linear contribution under bias due to BPVE, and ii) a maximum of photogenerated current in correspondence to the polarization switching bias. This is in agreement with recent photopolarization measurements on similar PMN-PT substrates,[47] where these combined effects were attributed to a net polarization increase when switching the FE state under illumination.

To evaluate the effects of illumination on the electrical properties of the heterostructure, photocurrent measurements were taken in the three polarization states under continuous 405 nm laser illumination at 800 mW cm^{-2} power. After a first period recorded with no light, the laser was switched on for 90 s, then switched off for the last 2 min. The resulting curves are shown in **Figure 5**a. In the pristine case, as the light was turned on, an increase in the sample current was observed due to BPVE, with a value of around 0.7 nA. Once turned off the laser, the initial state was sharply restored. On the other hand, slow dynamics with opposite trends were measured in polarized state. As the light was switched on, a photocurrent peak of opposite sign (positive for P_{down}, negative for P_{up}) appeared, exponentially decaying toward a steady value comparable to the pristine one. Once switched off the illumination, a similar transient effect, but opposite in sign, was observed for both cases, with a relaxation time quite comparable to the one under illumination. These transient effects were observed for all intensities of illumination (see Figure S6, Supporting Information), and are signature of the presence of a net electric dipole after sample polarization. As it will be shown in Section 2.5, once polarized the majority of the domains align along the [001] direction, with an electric dipole pointing up or down according to the polarization state (Figure 5b). When the light illumination is off, no free carriers are present in conduction band of the FE material, but only accumulated charges on the electrodes due to the net electric dipole of the polarized substrate. According to the common definition of BPVE as the generation of a steady photocurrent and above-bandgap photovoltage in a single-phase homogeneous material lacking inversion symmetry,[52] we adopt it in the discussion of the observed steady photocurrent, in spite of the lack of direct evidence of a photovoltage but supported by the photostrictive effects detected on Ni. Therefore, after turning on the light, BPVE induces the generation of free charges in the conduction band that reduce the resistance. In case of polarized substrate, the charges accumulated on the

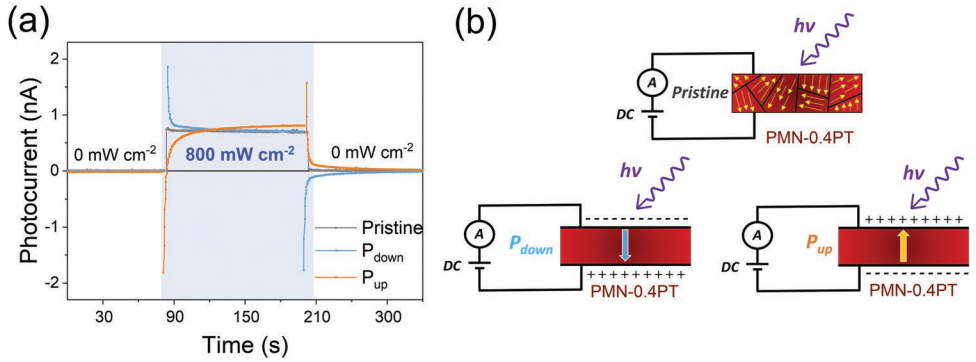

Figure 5. a) Photocurrent evolution of the PMN-PT/Ni heterostructure as a function of time for three different polarization states (pristine, P_{down} and P_{up}) under 1 V bias. After the 90 s with no light, the sample is illuminated by the 405 nm continuous laser at 800 mW cm^{-2} power (blue area) for 90 s. When the laser is switched off, the photocurrent was measured for additional 60 s. b) Schematic representation of the photocurrent measurements in the three PMN-PT ferroelectric configurations. In pristine state, randomly oriented ferroelectric domains give no net static charges, while for P_{down} and P_{up} states net accumulated charges are present on the top and bottom electrode of PMN-PT. Under illumination, the filling of the conduction band with photogenerated current induces a variation of the resistance and results, in the case of polarized PMN-PT, in the discharging of the accumulated charges.

top and bottom electrodes due to poling effect attract these photogenerated charge carriers, creating a depletion layers across the electrodes.[53] This will further trigger the depolarization field in the material, having opposite polarity with respect to the ferroelectric dipole. The transient between the two steady states (high resistance under no light, lower resistance under illumination due to photocurrent) is the signature of the current flow from the accumulated charges on the electrodes, whose sign is dependent on the dipole direction (P_{up} or P_{down}). Once the illumination is turned off, the BPVE will be stopped because of non-availability of new free charges. A second transient of opposite sign takes place at this stage, with the recovery of the net electric dipole and its accumulated charges at the electrodes. For both polarizations, the photocurrent reached its steady state after around 45 s, signature of a slow dynamic in the discharging of the substrate. This time dependence of polarized FE is rarely reported in literature,[38] and is an additional proof of the structural order compared to the pristine case, where this dynamic was not detected due to the disordered FE domains, whose internal electric field average to zero (see the schematics in Figure 5b). Similar transient effects upon illumination have been attributed to a coupled mechanism of photovoltaic and pyroelectric effects.[54–56] In our case, the lack of transient currents for pristine PMN-PT at 405 nm illumination and for the polarized case under well below-band gap illumination (658 nm) indicates the lack of any detectable pyroelectric contribution (Figure S7, Supporting Information). Finally, both Au/Ni and AuRh electrodes play a role in the built-in electric field upon illumination, balancing the depolarization field of the PMN-PT with their internal electric fields at the interfaces.[57]

Finally, we underline that the steady intensity of the photocurrent under illumination is almost identical in the three cases. This is important because it means that the amount of BPVE is unmodified after polarization, while in the following we will see that the photostrictive effects on interfacial magnetostrictive Ni are reduced once polarized. The polarization switching of the substrate was done without illumination for all the magnetic characterizations discussed in the article.

2.4. Light-Induced Effects on the Magnetic Properties of Polarized PMN-PT/Ni

Similarly, to the pristine case, the magnetic response under illumination was evaluated by combining MOKE and XMCD measurements for both polarization states. **Figure 6** shows the data for P_{down} (Figure 6a,c) and P_{up} (Figure 6b,d), without and with light illumination. As it can be clearly seen, for both polarizations the effects of light illumination are reduced with respect to the pristine state. From MOKE, we see an increase in the coercive field with no light for both P_{down} and P_{up} cases, being 43 and 41 Oe respectively, larger values compared to the pristine one (see Figure 2b). We attribute this increase to the structural modifications occurred in the substrate (see Section 2.5), which lead to a different interfacial strain on magnetostrictive Ni and its consequent changes in magnetocrystalline anisotropy.[58] Under illumination, the effects are much weaker (around 41 Oe for P_{down} and 39 Oe for P_{up}), in comparison to what observed in pristine. Correspondingly, almost no detectable effect of light illumination was found from XMCD measurements (see Figure 6c,d). In particular, the dichroic intensity at L_3 edge results slightly increased in the case of P_{down} (from (6.1 ± 0.2)% to (6.4 ± 0.2)%), and almost constant for P_{up} ((8.1 ± 0.2)%), while the noise of the measurements on the L_2 edge did not allow to properly evaluate the magnetic orbital and magnetic moments, whose variation, if any, is below our sensitivity.

2.5. PMN-PT Structural Characterization

The structural properties of pristine and electrically polarized PMN-PT substrates were determined by means of x-ray diffraction (XRD) using Cu-Kα radiation. In case of PMN-0.4PT, the structure lies near the morphotropic phase boundary and is expected to be tetragonal at room temperature.[33]

Figure 7 represents the XRD θ–2θ scan of (002) peak for the pristine and P_{down} polarized substrate. Our group previously reported that both the P_{up} and P_{down} states are structurally

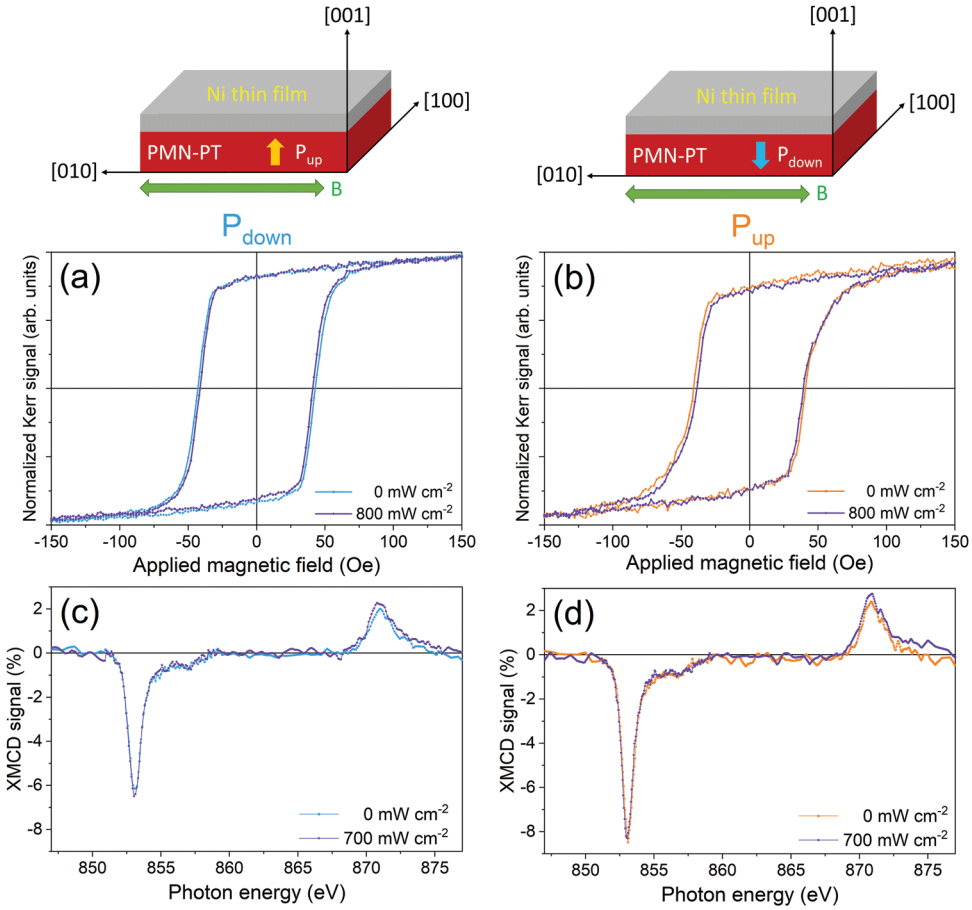

Figure 6. a,b) MOKE hysteresis loops of the electrically polarized PMN-PT/Ni heterostructure under 0 and 800 mW cm^{-2} illumination in the two polarization states, and c,d) XMCD dichroic signal at Ni $L_{2,3}$ edges under 0 and 700 mW cm^{-2}, with the magnetic field applied along the [010] axis of the substrate (as can be seen in the sketch at the top of figure).

identical.[13] The pristine state presents a combination of out-of-plane (002) and in-plane (020)/(200) domains. After setting the polarization to P_{down}, i.e., along the out-of-plane direction, the contribution of the (020)/(200) peak becomes smaller, changing the ratio between the two peaks. These results show a variation of the domain composition between pristine and polarized substrate,[58,59] giving a complementary information to the photocurrent measurements. While the charging/discharging under illumination (Figure 5b) confirmed the charge accumulation on the electrodes of the polarized states, here θ–2θ scans, and complementary 2D reciprocal space maps shown in Figure S8 (Supporting Information), show that pristine substrate presented a fraction of in-plane oriented domains, which vanished after setting the polarization. Our magnetic and spectroscopic characterization show how these domains are the main responsible of the photostrictive response under illumination, responsible of the effects observed in the Ni overlayer.

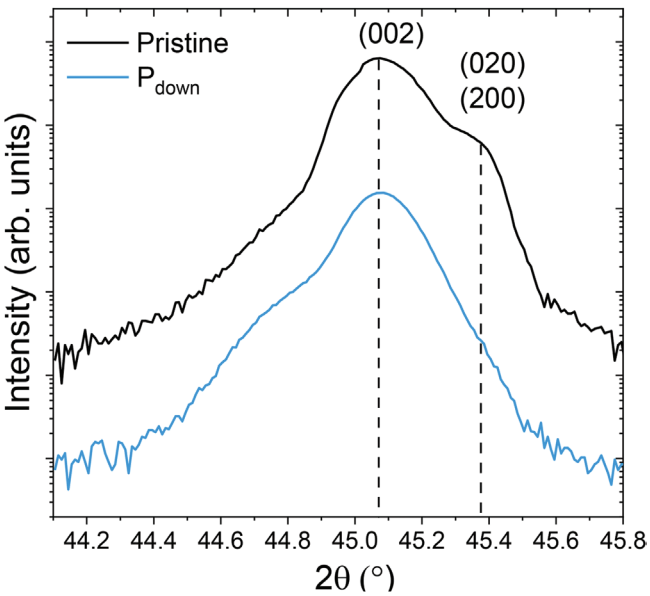

Figure 7. XRD θ–2θ scan of PMN-0.4PT substrate for pristine and electrically poled (P_{down}) case (out-of-plane polarized).

3. Conclusion

By combining electrical, structural, magnetic, and spectroscopic characterizations, we showed how light illumination

modifies significantly the properties of PMN-0.4PT substrate, and how these changes affect the magnetic properties of interfacial Ni layer. Photocurrent measurements and $I(E)$ curves showed the photocurrent generation via BPVE, whose intensity is maximized when illuminated by light wavelengths around the bandgap energy. When polarized out-of-plane, the photocurrent leads to the charging/discharging of the electrodes, consistently with the presence of a net electric dipole. The effects of the substrate induced photostriction were observed also by measuring the properties of the interfacial magnetostrictive Ni layer. In the pristine state, when the domain population is largely set in-plane, the magnetic coercive field of Ni was reduced by 45% under illumination. Sum rule analysis of the XMCD spectra showed an increase of the Ni orbital moment under these circumstances, indicating a different electronic environment of Ni as driven by the interfacial photostriction. Once polarized, the coercive field increased significantly for both the polarization states, and the influence of illumination became almost negligible. Both effects are connected to the PMN-PT structural changes after polarization, with the out-of-plane domains being less sensitive to photostriction. These results correlate with each other the effects of light illumination on both FE and FM parts of the heterostructure, allowing to link the modifications on the former to the changes on the latter.

4. Experimental Section

Sample Preparation: A 10 nm thick Nickel layer was grown by e-beam evaporation on top of an unpolarized one-sided polished (001) PMN-0.4PT 2.5 × 2.5 mm^2 substrate of 0.5 mm thickness from SurfaceNet GmbH supplier, at a base pressure below 1×10^{-7} mbar. At the same pressure, the prepared sample was then capped by an 8 nm thick Au layer from the top to prevent Ni oxidation and acting as the top electrode for the electrical measurements. The unpolished backside of the substrate was then coated with a 5 nm thick AuRh layer using magnetron sputtering, acting as backside electrode in the electrical measurements. All the depositions were carried out at the room temperature.

Electrical Measurements: The two electrodes were contacted by using specially designed Ultra High Vacuum (UHV) compatible sample holders,[59] using a gold wire connection for the top electrode and silver paste on the backside. $I(E)$ and photocurrent measurements were taken using a Keithley 6485 picoammeter/voltage source. Measurements were recorded both in absence and presence of laser illumination. A 405 nm wavelength continuous laser source with variable power (0–800 mW cm^{-2}) from RGB Lasersystems was used to illuminate the whole sample surface.

Photocurrent measurements were taken by recording the amount of current flowing through the thickness of the sample under the application of 1 V steady DC voltage, modulating the laser intensity during the measurement.

The $I(E)$ curves were performed by recording the current flowing through the thickness of the sample under the application of an out-of-plane voltage of ±300 V (6 kV cm^{-1}). The set of measurements was taken for both in air for MOKE and in UHV conditions for in situ XAS/XMCD characterizations, showing no differences in the electrical response.

OPA Setup: The laser source is based on a Yb:KGW integrated femtosecond laser system (PHAROS, Light Conversion), producing around 300 fs pulses at 1030 nm, with a repetition rate of 50 kHz, an average power of 20 W and a maximal energy-per-pulse equal to 400 µJ. The laser seeds an optical parametric amplifier (OPA), with a tunable output in the range of 210–2500 nm. A fixed pinhole ensures the same optical spot dimension on the sample, and all the used wavelengths have the same average power after the pinhole: in this way the fluence on the sample is the same for every used wavelength.

The photocurrent scanning measurements were performed by using an ORPHEUS collinear Optical Parametric Amplifier (OPA) tool manufactured by Light Conversion company.

MOKE Measurements: The magnetic hysteresis loops have been measured by longitudinal MOKE, using an *s*-polarized 658 nm wavelength laser of 8 mW power, with a laser spot of about 500 μm^2. Coercive field was evaluated as the averaged half width hysteresis loops at zero magnetization, averaging both the negative and positive sides of the loop. The sample was then illuminated by the 405 nm laser with normal incidence to the sample surface. The set of measurements was taken in the pristine state and repeated after switching the FE polarization without removing the sample from the measurement stage.

XAS/XMCD Measurements: XAS and XMCD spectra at Ni $L_{2,3}$ edges were taken at the APE-HE beamline of the Elettra synchrotron radiation facility in Trieste.[60] The specifically designed sample holders allowed for switching the FE polarization state without removing the sample from the measuring stage. All spectra were measured in total electron yield (TEY) mode by normalizing the intensity of the sample current to the incident photon flux current at each energy value. The sample surface was kept at 45° with respect to the incident beam. XMCD measurements was performed at magnetic remanence, after applying an in-plane alternating magnetic field pulse of ±300 Oe at every measured photon energy value. The recorded XMCD signal was then normalized to the sum of the two XAS for positive and negative magnetic field values. All the XMCD signals were shown in %, taking into consideration the angle of 45° between the photon angular momentum and the in-plane magnetization, as well as the 75% circular polarization degree of light. To illuminate the sample under measurements, the 405 nm laser was placed in front of a UV transparent view-port, impinging the sample from front with a measured irradiance of 700 mW cm^{-2} on the sample, the maximum can be reached.

Structural Characterizations: XRD measurements were performed with X'Pert PANalytical instrument available at the NFFA-Trieste facility. The monochromatic Cu-kα (λ = 1.54056 Å) radiation was used in the setup in the Bragg–Brentano configuration at room temperature. The structure was observed using high-resolution mode with incident optics composed of a 4-bounce Ge(220) to select only Cu-K α_1 line.

Supporting Information

Supporting Information is available from the Wiley Online Library or from the author.

Acknowledgements

This work was performed in the framework of the Nanoscience Foundry and Fine Analysis (NFFA-MUR Italy Progetti Internazionali) project (www.trieste.NFFA.eu).

Conflict of Interest

The authors declare no conflict of interest.

Data Availability Statement

The data that support the findings of this study are available from the corresponding author upon reasonable request.

Keywords

ferroelectrics and multiferroics, information storage technology, light-modified magnetism, multiferroic heterostructures, photostriction and photovoltaics

Received: June 15, 2022
Revised: October 4, 2022
Published online: November 14, 2022

[1] M. Fiebig, T. Lottermoser, D. Meier, M. Trassin, *Nat. Rev. Mater.* **2016**, *1*, 16046.
[2] M. Trassin, *J. Phys.: Condens. Matter* **2016**, *28*, 033001.
[3] C. A. Fernandes Vaz, U. Staub, *J. Mater. Chem. C* **2013**, *1*, 6731.
[4] M. Fiebig, *J. Phys. D: Appl. Phys.* **2005**, *38*, R123.
[5] W. Eerenstein, N. D. Mathur, J. F. Scott, *Nature* **2006**, *442*, 759.
[6] J. P. Velev, S. S. Jaswal, E. Y. Tsymbal, *Philos. Trans. R. Soc., A* **2011**, *369*, 3069.
[7] J.-M. Hu, L.-Q. Chen, C.-W. Nan, *Adv. Mater.* **2016**, *28*, 15.
[8] C. Song, B. Cui, F. Li, X. Zhou, F. Pan, *Prog. Mater. Sci.* **2017**, *87*, 33.
[9] M. Liu, N. X. Sun, *Philos. Trans. R. Soc., A* **2014**, *372*, 20120439.
[10] F. Matsukura, Y. Tokura, H. Ohno, *Nat. Nanotechnol.* **2015**, *10*, 209.
[11] P. B. Meisenheimer, S. Novakov, N. M. Vu, J. T. Heron, *J. Appl. Phys.* **2018**, *123*, 240901.
[12] J.-M. Hu, C.-W. Nan, *APL Mater.* **2019**, *7*, 80905.
[13] G. Vinai, F. Motti, V. Bonanni, A. Y. Petrov, S. Benedetti, C. Rinaldi, M. Stella, D. Cassese, S. Prato, M. Cantoni, G. Rossi, G. Panaccione, P. Torelli, *Adv. Electron. Mater.* **2019**, *5*, 1900150.
[14] F. Motti, G. Vinai, V. Bonanni, V. Polewczyk, P. Mantegazza, T. Forrest, F. Maccherozzi, S. Benedetti, C. Rinaldi, M. Cantoni, D. Cassese, S. Prato, S. S. Dhesi, G. Rossi, G. Panaccione, P. Torelli, *Phys. Rev. Mater.* **2020**, *4*, 114418.
[15] V. Iurchuk, D. Schick, J. Bran, D. Colson, A. Forget, D. Halley, A. Koc, M. Reinhardt, C. Kwamen, N. A. Morley, M. Bargheer, M. Viret, R. Gumeniuk, G. Schmerber, B. Doudin, B. Kundys, *Phys. Rev. Lett.* **2016**, *117*, 107403.
[16] W. Wang, J. Li, H. Liu, S. Ge, *Adv. Sci.* **2021**, *8*, 2003074.
[17] I. Tatsuzaki, K. Itoh, S. Ueda, Y. Shindo, *Phys. Rev. Lett.* **1966**, *17*, 198.
[18] R. Pandey, G. Vats, J. Yun, C. R. Bowen, A. W. Y. Ho-Baillie, J. Seidel, K. T. Butler, S. Il Seok, *Adv. Mater.* **2019**, *31*, 1807376.
[19] T. Choi, S. Lee, Y. J. Choi, V. Kiryukhin, S.-W. Cheong, *Science* **2009**, *324*, 63.
[20] S. Y. Yang, J. Seidel, S. J. Byrnes, P. Shafer, C.-H. Yang, M. D. Rossell, P. Yu, Y.-H. Chu, J. F. Scott, J. W. Ager, L. W. Martin, R. Ramesh, *Nat. Nanotechnol.* **2010**, *5*, 143.
[21] F. Wang, S. M. Young, F. Zheng, I. Grinberg, A. M. Rappe, *Nat. Commun.* **2016**, *7*, 10419.
[22] B. Kundys, *Appl. Phys. Rev.* **2015**, *2*, 011301.
[23] K. Uchino, M. Aizawa, S. Nomura, *Ferroelectrics* **1985**, *64*, 199.
[24] P. S. Brody, *Ferroelectrics* **1983**, *50*, 27.
[25] B. Kundys, M. Viret, D. Colson, D. O. Kundys, *Nat. Mater.* **2010**, *9*, 803.
[26] B. Kundys, M. Viret, C. Meny, V. Da Costa, D. Colson, B. Doudin, *Phys. Rev. B: Condens. Matter Mater. Phys.* **2012**, *85*, 092301.
[27] P. Poosanaas, A. Dogan, S. Thakoor, K. Uchino, *J. Appl. Phys.* **1998**, *84*, 1508.
[28] Z. Jin, Y. Xu, Z. Zhang, X. Lin, G. Ma, Z. Cheng, X. Wang, *Appl. Phys. Lett.* **2012**, *101*, 242902.
[29] H. Wen, P. Chen, M. P. Cosgriff, D. A. Walko, J. H. Lee, C. Adamo, R. D. Schaller, J. F. Ihlefeld, E. M. Dufresne, D. G. Schlom, P. G. Evans, J. W. Freeland, Y. Li, *Phys. Rev. Lett.* **2013**, *110*, 37601.
[30] C. Paillard, S. Prosandeev, L. Bellaiche, *Phys. Rev. B* **2017**, *96*, 45205.
[31] A. J. Joseph, N. Sinha, S. Goel, A. Hussain, B. Kumar, *Arabian J. Chem.* **2020**, *13*, 2596.
[32] Z.-W. Yin, H.-S. Luo, P.-C. Wang, G.-S. Xu, *Ferroelectrics* **1999**, *229*, 207.
[33] Y. Guo, H. Luo, D. Ling, H. Xu, T. He, Z. Yin, *J. Phys. Condens. Matter* **2003**, *15*, L77.
[34] X. Wan, H. L. W. Chan, C. L. Choy, X. Zhao, H. Luo, *J. Appl. Phys.* **2004**, *96*, 1387.
[35] X. Wan, H. Xu, T. He, D. Lin, H. Luo, *J. Appl. Phys.* **2003**, *93*, 4766.
[36] C. He, F. Wang, D. Zhou, X. Zhao, D. Lin, H. Xu, T. He, H. Luo, *J. Phys. D: Appl. Phys.* **2006**, *39*, 4337.
[37] Y. H. Bing, R. Guo, A. S. Bhalla, *Ferroelectrics* **2000**, *242*, 1.
[38] A. Makhort, R. Gumeniuk, J.-F. Dayen, P. Dunne, U. Burkhardt, M. Viret, B. Doudin, B. Kundys, *Adv. Opt. Mater.* **2022**, *10*, 2102353.
[39] X. Zhang, X. Guo, B. Cui, J. Yun, J. Mao, Y. Zuo, L. Xi, *Appl. Phys. Lett.* **2020**, *116*, 132405.
[40] W. Eerenstein, M. Wiora, J. L. Prieto, J. F. Scott, N. D. Mathur, *Nat. Mater.* **2007**, *6*, 348.
[41] Y. Wang, F. Wang, S. W. Or, H. L. W. Chan, X. Zhao, H. Luo, *Appl. Phys. Lett.* **2008**, *93*, 113503.
[42] S. Y. Chen, D. H. Wang, Z. D. Han, C. L. Zhang, Y. W. Du, Z. G. Huang, *Appl. Phys. Lett.* **2009**, *95*, 22501.
[43] M. Zheng, H. Ni, X. Xu, Y. Qi, X. Li, J. Gao, *Phys. Rev. Appl.* **2018**, *9*, 44039.
[44] W. J. Hu, Z. Wang, W. Yu, T. Wu, *Nat. Commun.* **2016**, *7*, 10808.
[45] Y. A. Genenko, J. Glaum, M. J. Hoffmann, K. Albe, *Mater. Sci. Eng., B* **2015**, *192*, 52.
[46] Z. Lü, K. Zhao, H. Liu, N. Zhou, H. Zhao, L. Gao, S. Zhao, A. Wang, *Chin. Opt. Lett.* **2009**, *7*, 1048.
[47] A. S. Makhort, F. Chevrier, D. Kundys, B. Doudin, B. Kundys, *Phys. Rev. Mater.* **2018**, *2*, 3.
[48] A. Dmitriyeva, V. Mikheev, S. Zarubin, A. Chouprik, G. Vinai, V. Polewczyk, P. Torelli, Y. Matveyev, C. Schlueter, I. Karateev, Q. Yang, Z. Chen, L. Tao, E. Y. Tsymbal, A. Zenkevich, *ACS Nano* **2021**, *15*, 14891.
[49] P. Gambardella, S. Rusponi, M. Veronese, S. S. Dhesi, C. Grazioli, A. Dallmeyer, I. Cabria, R. Zeller, P. H. Dederichs, K. Kern, C. Carbone, H. Brune, *Science* **2003**, *300*, 1130.
[50] C. T. Chen, Y. U. Idzerda, H.-J. Lin, N. V. Smith, G. Meigs, E. Chaban, G. H. Ho, E. Pellegrin, F. Sette, *Phys. Rev. Lett.* **1995**, *75*, 152.
[51] W. L. O'Brien, B. P. Tonner, *Phys. Rev. B* **1994**, *50*, 12672.
[52] L. Z. Tan, F. Zheng, S. M. Young, F. Wang, S. Liu, A. M. Rappe, *NPJ. Comput. Mater.* **2016**, *2*, 16026.
[53] D. G. Popescu, M. A. Huşanu, L. Trupină, L. Hrib, L. Pintilie, A. Barinov, S. Lizzit, P. Lacovig, C. M. Teodorescu, *Phys. Chem. Chem. Phys.* **2015**, *17*, 509.
[54] A. Zenkevich, Y. Matveyev, K. Maksimova, R. Gaynutdinov, A. Tolstikhina, V. Fridkin, *Phys. Rev. B* **2014**, *90*, 161409.
[55] A. M. Glass, D. von der Linde, T. J. Negran, *Appl. Phys. Lett.* **1974**, *25*, 233.
[56] N. Ma, K. Zhang, Y. Yang, *Adv. Mater.* **2017**, *29*, 1703694.
[57] Z. Lu, P. Li, J. Wan, Z. Huang, G. Tian, D. Pan, Z. Fan, X. Gao, J. Liu, *ACS Appl. Mater. Interfaces* **2017**, *9*, 27284.
[58] G. Vinai, B. Ressel, P. Torelli, F. Loi, B. Gobaut, R. Ciancio, B. Casarin, A. Caretta, L. Capasso, F. Parmigiani, F. Cugini, M. Solzi, M. Malvestuto, R. Ciprian, *Nanoscale* **2018**, *10*, 1326.
[59] F. Motti, G. Vinai, A. Petrov, B. A. Davidson, B. Gobaut, A. Filippetti, G. Rossi, G. Panaccione, P. Torelli, *Phys. Rev. B* **2018**, *97*, 94423.
[60] G. Panaccione, I. Vobornik, J. Fujii, D. Krizmancic, E. Annese, L. Giovanelli, F. Maccherozzi, F. Salvador, A. De Luisa, D. Benedetti, A. Gruden, P. Bertoch, F. Polack, D. Cocco, G. Sostero, B. Diviacco, M. Hochstrasser, U. Maier, D. Pescia, C. H. Back, T. Greber, J. Osterwalder, M. Galaktionov, M. Sancrotti, G. Rossi, *Rev. Sci. Instrum.* **2009**, *80*, 043105.